

## Multi-stimuli Responsive Composite for heavy metal detection Based on Mesoporous Silica and Polyelectrolyte Brush

Long Wu<sup>1,2</sup>, Zan Ge<sup>1</sup>, Wei Li<sup>3</sup>, Feng Chen<sup>1,2,\*</sup>, Zeping Zhou<sup>2,\*</sup>

<sup>1</sup> Surfactants Key Enterprise Laboratory of Zhejiang Province, Zanyu Technology Group Co., LTD., Hangzhou 310030, China

<sup>2</sup> College of Materials Science and Engineering, Zhejiang University of Technology, Hangzhou 310014, China

<sup>3</sup> Nantong Acetic Acid Chemical Co., Ltd., Nantong 226009, China

\*E-mail: [chenf@zjut.edu.cn](mailto:chenf@zjut.edu.cn)

Received: 17 July 2019 / Accepted: 21 November 2019 / Published: 30 November 2019

Heavy metals are mostly non-degradable toxic substances, which are easy to be absorbed and enriched by organisms in the ecosystem, resulting in accumulation of the human body and difficult to be discharged. The electrochemical sensor is an effective method to detect heavy metal ions. Based on mesoporous silica, a multi-responsive block polymer brush PMAzo-PDMAEMA-SBA-15 was prepared by SI-RAFT method. Then the polymer brush was prepared into an electrochemical sensor to detect  $[Fe(CN)_6]^{3-}$ ,  $Cu^{2+}$ ,  $Cd^{2+}$  by CV test, and the detection limit is about  $1.0 \times 10^{-7} \sim 2 \times 10^{-6}$  mol/L. It was found that the linear relationship between peak reduction current and metal ion concentration is excellent so the electrochemical sensors can be used for quantitative detection of ions. In addition, we also tested the performance of the sensor under the different environments such as pH, temperature and ultraviolet light, and found that sensitivity and detection limit of the sensor would greatly increase at low pH and high temperature, and the UV-visible light could be used as the control switch of the sensor.

**Keywords:** Polyelectrolyte/mesoporous Silica, SI-RAFT, Environmental Response, Electrochemical Sensors, Metal Ions

### 1. INTRODUCTION

With the development of society, the continuous expansion of metal resources has caused a large number of heavy metal pollution [1,2]. The heavy metal element refers to a metal element having an atomic mass between 63.5 and 200.6, and the relative density is above 5 g/cm<sup>3</sup>, mainly includes copper, cadmium, lead, nickel, and so on. Most of the heavy metals are non-degradable toxic substances, which are easily absorbed and enriched by organisms in the ecosystem, and eventually

accumulated in organisms, endangering life and health [3,4,5]. Therefore, heavy metal pollution has the characteristics of strong toxicity, enrichment and durability. The detection method of heavy metal ions with simple operation, low-cost and efficiency has been a research hotspot in recent years [6-9].

The electrochemical sensor method is a convenient, rapid and sensitive detection method [10-13], which can be used for the detection of heavy metal ions [14,15]. The testing performance of the electrochemical sensor depends on the specific surface area of the chemically modified electrode and the chelating group. Nanoporous materials have received great attention and have been used in various fields [16-25]. Mesoporous silica is a new type of porous nanomaterial with controllable pore size, uniform size, and high specific surface area. It is widely used in catalysis [26-28], sensing [29-31], biomedicine [32-35], drug delivery [36-39] and other fields. Its pore size is uniformly controllable in the range of 2-50 nm and has a large pore volume and specific surface area (up to 700 m<sup>2</sup>/g) [40]. Mesoporous silica SBA-15 has better biocompatibility and chemical stability and is highly concerned by researchers [41-45].

Surface reversible addition fragmentation chain transfer polymerization (SI-RAFT) is a controlled active radical polymerization. Dithioesters or trithioesters with high chain transfer constants are usually used as chain transfer agents to design polymers with special structures, such as hyperbranched combs and stars [46]. With mild reaction conditions, SI-RAFT can be used in a variety of polymerization processes, without metal atomic residues, and with narrow molecular weight distribution. In particular, SI-RAFT is suitable for various monomers and can be used for monomers with specific groups, such as carboxyl or dialkyl amine groups [47-49].

Hence we prepared PMAzo-PDMAEMA-SBA-15 multiresponse block polymer brush with SBA-15 as the substrate by SI-RAFT method. By controlling the feed ratio and reaction conditions, polymer brushes with different block ratios were designed and we studied their compositions and structures. Electrochemical sensors with multiple responsiveness were prepared using the above composite materials, and then we studied the detection performance of [Fe(CN)<sub>6</sub>]<sup>3-</sup>, Cu<sup>2+</sup>, Cd<sup>2+</sup>. And we further analyzed influence of different environments on the sensor. The results of cyclic voltammetry showed there was a linear relationship between the reduction peak current and the concentrations of [Fe(CN)<sub>6</sub>]<sup>3-</sup>, Cu<sup>2+</sup> and Cd<sup>2+</sup>, with a very good linear correlation and a low detection limit. And the detection is more sensitive and the detection limit is lower in the high temperature and low pH environment. This indicates that the electrochemical sensor can quantitatively detect [Fe(CN)<sub>6</sub>]<sup>3-</sup>, Cu<sup>2+</sup>, Cd<sup>2+</sup>, which has certain application prospects.

## 2. EXPERIMENTAL

### 2.1. Materials

All chemical agents were purchased from Aladdin Chemistry Co. Ltd, China and without any further purification, including silane coupling agent 3-aminopropyltriethoxysilane (APTES), toluene, 1-(3-dimethylaminopropyl)-3-ethylcarbodiimide hydrochloride (EDC), *N*-hydroxysuccinimide (NHS), *N,N*-dimethyl aminoethyl methacrylate (DMAEMA), 2,2-azobisisobutyronitrile (AIBN),

dimethylacetamide (DMAc), acrylamido azobenzene (modified azo, referred to MAzo), methanol, 3-aminopropyltriethylsilane, potassium ferricyanide, potassium ferrocyanide, azobisisobutyronitrile, methyl trioctyl ammonium chloride, *N*-dodecyl mercaptan, acryloyl chloride, copper nitrate, cadmium nitrate, absolute alcohol, trichloromethane, sodium hydroxide, acetone, *p*-aminoazobenzene, carbon disulfide, potassium chloride, quinol, triethylamine, isopropanol. Mesoporous silica (SBA-15), which had an average diameter of 8 nm, was purchased from XFNANO Materials Tech Co. Ltd, China.

## 2.2. Material preparation process

Mesoporous silica SBA-15, silane coupling agent (APTES) and toluene were placed in a round bottom flask, reacted at 100 °C for 24 hours, centrifuged and vacuum dried, named NH<sub>2</sub>-SBA-15. Add NH<sub>2</sub>-SBA-15, the RAFT initiator trithiocarbonate (DDMAT) [47,50] to deionized water, and then add excess EDC, NHS, sequentially. The reaction was stirred at room temperature for 24 hours, centrifuged, and vacuum dried, the product was named RAFT-SBA-15.

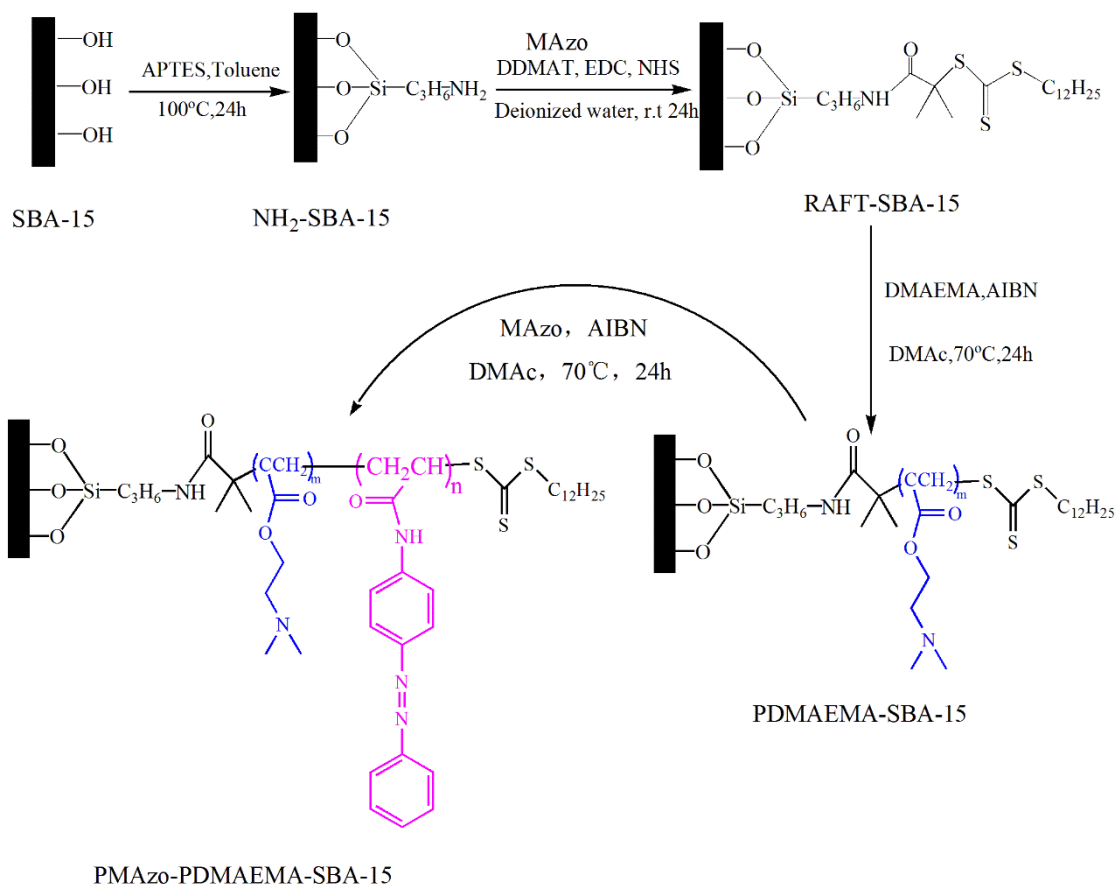


**Figure 1.** The synthesis protocol of PMAz-PDMAEMA-SBA-15 hybrid nanocomposites.

Combining the TG results of SBA-15, NH<sub>2</sub>-SBA-15 and RAFT-SBA-15, the surface grafting ratio of the chain transfer agent DDMAT can be calculated. Then RAFT-SBA-15, DMAEMA, AIBN and DMAc were added to the flask, and the reaction system was heated in an oil bath under nitrogen

atmosphere, and reacted at 70 °C for 24 hours, and the flask was placed in ice water to stop the reaction. The product after centrifugation was named PDMAEMA-SBA-15. To synthesize to block polymer brushes, PDMAEMA-SBA-15, MAzo, AIBN and DMAc were added to the flask, and reacted under nitrogen for 24 hours at 70 °C. The tube was placed in ice water to stop the reaction. After centrifugation, it was vacuum dried and named PMAzo-PDMAEMA-SBA-15.

### 2.3 Characterization

The X-ray photoelectron spectroscopy (XPS) was investigated using an X-ray photoelectron spectroscopy analyzer (Axisaxis Ultra ltra (DLD), Shimadzu). Binding energy (BE) ratio is calibrated with C-H C1s (284.8 eV). Thermogravimetric analysis (TGA) was investigated using a thermogravimetric analyzer (SDTQ600, USA). All samples were heated from room temperature to 800 °C at a heating speed of 10 °C/min under nitrogen atmosphere. The product was subjected to nitrogen adsorption and desorption analysis using a specific surface and porosity analyzer (ASAP2020C+). The product was pre-degassed in a degassing station under vacuum for 12 hours, and then the nitrogen adsorption and desorption curves and pore size distribution curves were tested at the analytical station in a liquid nitrogen atmosphere.

### 2.4 Electrochemical performance analysis

Cyclic voltammetry curves of electrochemical workstations (RST4800) were used to test the performance and environmental response of the characterization samples for different ions. The PMAzo-PDMAEMA SBA-15 and silane coupling agent were dissolved in a small amount of alcohol, coated on a graphite sheet, connected with a copper wire, and the joint was fixed with the raw tape and the sealant, dried to be tested [50,51]. The test was carried out using a three-electrode system. The self-made nanocomposite electrode was the working electrode, the platinum plate electrode was the counter electrode, the saturated calomel electrode (SCE) was the reference electrode, and the support solution was 0.1mol/L KCl solution [52,53]. The scanning voltage is -0.2- 0.6v.

## 3. RESULTS AND DISCUSSION

### 3.1 Characterizations of hybrid nanocomposite

In order to demonstrate the successful graft of the polymer brush on mesoporous silica, the surface elemental composition of PMAzo-PDMAEMA-SBA-15 was analyzed by XPS analysis and the results were shown in Fig.2 (a). As can be seen from the Fig, the characteristic peak at 285 eV is the peak of C1s; the characteristic peak at 399 eV is the peak of N1s; the characteristic peak at 532 eV is the peak of O1s; the characteristic peak at 152 eV is the peak of Si2s; the characteristic peak at 101 eV is the peak of Si2p, and the characteristic peak at 22 eV is the peak of O2s. By combining the structural formula of block polymer brush, we can determine the successful production of the target

product PMAzo-PDMAEMA-SBA-15. In the polymer brush, the content of C is 84.96%, the content of N is 15.04%. The theoretical values of the C and N contents can be calculated from the structural formula of the polymer brush. For the polymer brush of  $D_{\text{polyMAzo}}$ :  $D_{\text{polyDMAEMA}} = 70:30$ , the theoretical value of the C content is 83.85%, and the theoretical value of the N content is 16.15%. The elemental analysis results of XPS are very close to the theoretical values, indicating that the composition ratio of each block is effectively controlled. The structure of the block polymer brush conforms to the theoretical design, and the multi-response nanocomposite has been successfully prepared.

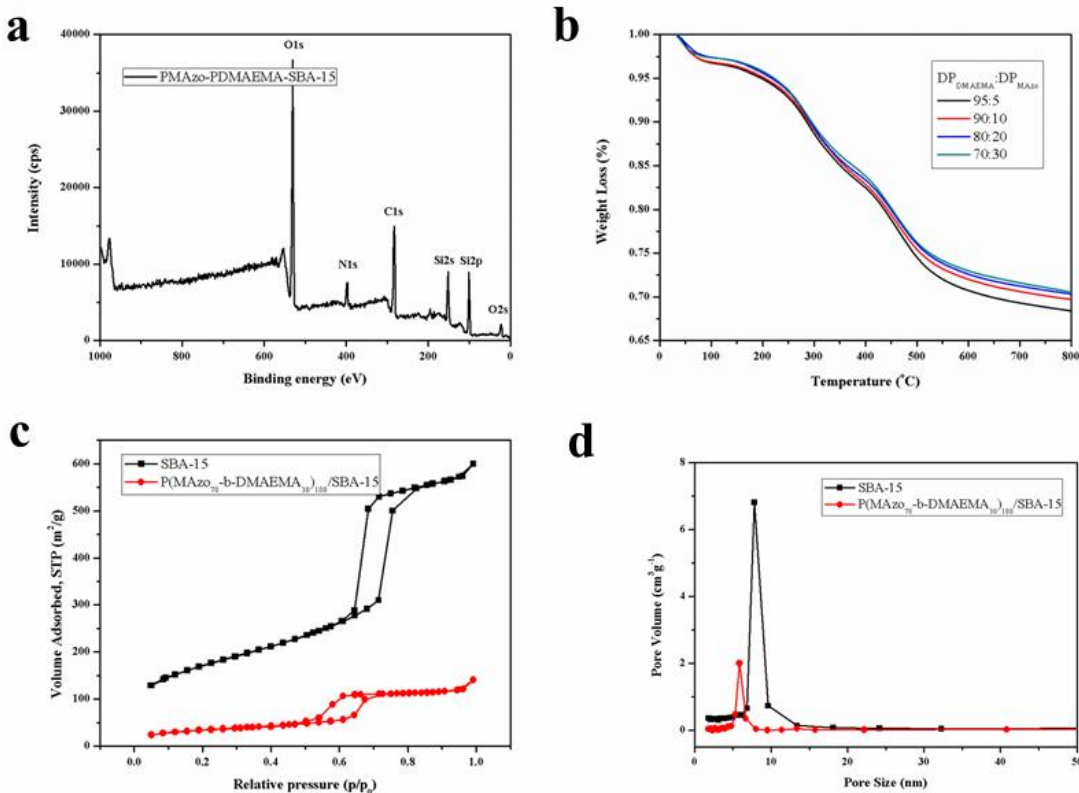


**Figure 2.** (a) XPS survey spectra of PMAzo-PDMAEMA-SBA-15; (b) TGA curves of PMAzo-PDMAEMA-SBA-15 scanning from room temperature to 800 °C at a scanning speed of 10 °C/min; (c) N<sub>2</sub> absorption/desorption isotherm of SBA-15 and PMAzo-PDMAEMA-SBA-15; (d) Pore size distribution of SBA-15 and PMAzo-PDMAEMA-SBA-15.

Fig.2 (b) is the TGA results of PMAzo-PDMAEMA-SBA-15 with different block ratios. It can be seen from the Fig that PMAzo-PDMAEMA-SBA-15 has a significant mass loss in the TGA test. The mass loss of the composite material is about 3% when the temperature is under 100 °C, this is the loss of a small amount of moisture contained in the sample. In 200 °C to 400 °C temperature range, the mass loss is about 16%, this is due to decomposition of the carbon chain in the sample and decomposition of groups such as C=O. Because of decomposition of benzene ring structure in composite materials, the mass loss is about 11% in the range of 400 to 500 °C. The final residual mass is about 70%, the remainder is mainly high temperature resistant substrate mesoporous silica in the

composite material and a small amount of polymer chain decomposition residual rearrangement carbon. At the same time, it was found that with the increase of polyMAzo proportion in the block polymer brush, the residual mass increased from 68.5% to 70.6%, which was due to the increase of benzene ring content in the composite material. The TGA results further proved that polymer brush prepared on mesoporous silicon was consistent with the theory.

The PMAzo-PDMAEMA-SBA-15 and SBA-15 were characterized by nitrogen adsorption desorption curve analysis. The results are shown in Fig.2 (c) and (d). As can be seen from the Fig, there is a significant hysteresis loop in the curve, and there is capillary condensation in the range of  $P/P_0$  of 0.5 to 0.8. According to the classification of international union of pure and applied chemistry (IUPAC), it belongs to the class IV curve so this composite material is a typical mesoporous material. This indicates that the specific surface area of nanocomposites modified by block polymer brush is reduced, but the original mesopore morphology is retained [49]. Fig.2 (d) shows the pore size distribution of SBA-15 and nanocomposites. As can be seen from the Fig, the pore size of nanocomposites modified by block polymer brush decreases. Table 1 is a specific data sheet for Brunauer Emmett Teller (BET) analysis of composite materials. As the proportion of PMAzo in the block polymer brush increases, the average pore size and specific surface area of the nanocomposite decrease, which is due to the increase of the proportion of large volume group MAzo in the polymer brush [49].

**Table 1.** Structural properties of SBA-15 and various PMAzo-PDMAEMA-SBA-15 samples

DP <sub>DMAEMA</sub> :DP <sub>MAzo</sub>	Pore Size <sup>a</sup> (nm)	Surface Area <sup>b</sup> (m <sup>2</sup> g <sup>-1</sup> )	Pore Volume (cm <sup>3</sup> g <sup>-1</sup> )
SBA-15	7.9	513.0	0.87
95:5	4.09	132.7	0.22
90:10	4.01	132.1	0.23
80:20	3.44	128.6	0.22
70:30	3.40	125.7	0.22

(a) The average pore size and pore volume were calculated by Barrett-Joyner-Halenda (BJH) method.

(b) The specific surface area was calculated by BET method.

### 3.2 Detection of heavy metal ions by hybrid nanocomposite electrode

Fig.3 (a) is the cyclic voltammogram (CV) curves of graphite electrode and self-made hybrid nanocomposite electrode in a 2 mM  $[\text{Fe}(\text{CN})_6]^{3-}$  solution at a scanning rate of 50 mV/s. As can be seen from the Fig.3, the redox peak current of the graphite electrode is large, the peak shape is not obvious and the redox peaks are asymmetric. Since the specific surface area of the multi-response electrode is very large, the structure of the block polymerization brush contains a large amount of active groups and conjugated structures which is conducive to the adsorption and reaction of ions on the electrode,

the redox peak is more obvious. These phenomena indicate that the nanocomposite electrode can be used for the CV analysis of ions.

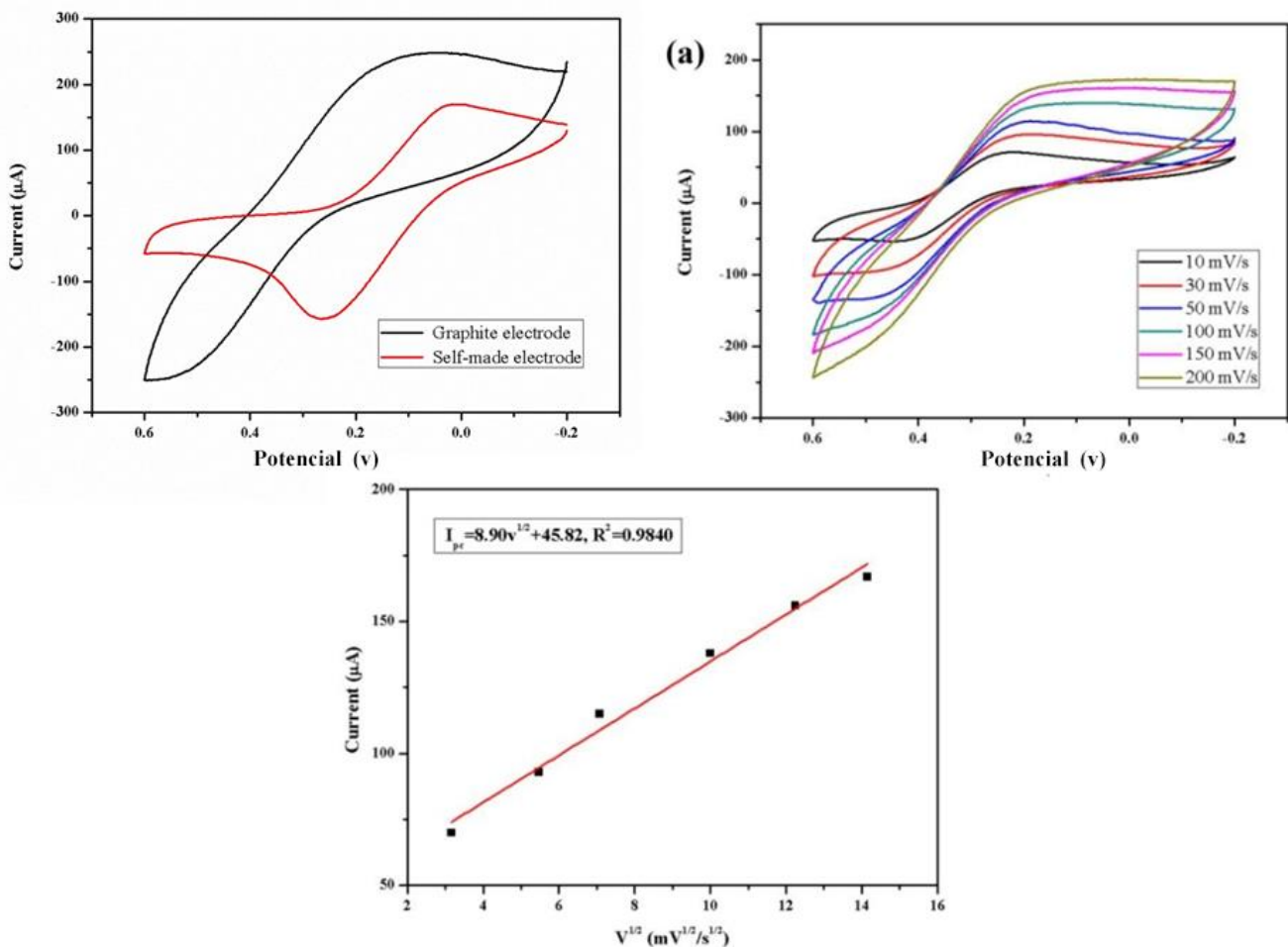


**Figure 3.** (a) CV curves of graphite and self-made multi-responsive electrode, with that the scanning rate is 50 mV/s and electrolyte is 2 mM  $[\text{Fe}(\text{CN})_6]^{3-}$  solution; (b) CV curves at different scan rates; (c) The relationship between the reduction peak current and the square root of scanning rate in the 1 mM  $[\text{Fe}(\text{CN})_6]^{3-}$  solution.

The CV curve of the multi-response composite electrode was tested at different scanning speeds in 1 mM  $[\text{Fe}(\text{CN})_6]^{3-}$  solution, and the results were shown in Fig.3 (b) and (c). As can be seen from Fig.3 (b), when the scanning speed is small, the  $[\text{Fe}(\text{CN})_6]^{3-}$  redox peak is obvious, and the cyclic voltammetry curve is also symmetrical. However, the small redox peak current value is not conducive to detection. With the increase of scanning speed (10~200 mV/s), the redox peak current of the cyclic voltammetry curve also increases. When the scanning rate is large, since the current also increases, the redox peak is not obvious, which is not conducive to detection. According to the test results, the scanning rate for ion detection in this chapter is 50 mV/s [54]. According to the Randles-Sevcik equation, the peak current  $i_p$  and the scanning speed  $V$  follow the following formula [55]:

$$i_p = 2.96 \times 10^5 n^{\frac{3}{2}} ACD^{\frac{1}{2}} V^{\frac{1}{2}} \quad (\text{Equation 1})$$

(n is the number of reaction electron transfer, A is the electrode active area, and C is the reactant concentration.)

The reduction peak current was linear to the 1/2 power of the velocity, and the results are shown in Fig.3 (c). It can be found that the two exhibit a good linear relationship, and the linear equations are  $i_{pc}=8.90v^{1/2}+45.82$  and  $R_2=0.9840$ , respectively.  $i_{pc}$  is the reduction peak current, the unit is uA;  $v^{1/2}$  is the 1/2 power of the scanning speed, and the unit is  $\text{mV}^{1/2}\cdot\text{s}^{-1/2}$ . Thus, the reduction process of  $[\text{Fe}(\text{CN})_6]^{3-}$  on the multi-response composite electrode is controlled by diffusion.

By CV test, a series of  $[\text{Fe}(\text{CN})_6]^{3-}$  solution with different concentrations were tested with a self-made multi-response composite electrode. The results are shown in Fig.4 (a), (b), (c) and (d). As can be seen from the figure, the cyclic voltammetry curve is symmetrical and the redox peak is obvious. When the initial potential (+ 0.6v) was scanned forward to the transition potential (-0.2v),  $[\text{Fe}(\text{CN})_6]^{3-}$  in the solution was reduced to  $[\text{Fe}(\text{CN})_6]^{4-}$ , resulting in a reduction current. The cathode peak potential  $E_{pc}$  was 0.05 V (vs. SCE); And from the negative scanning of the transition potential to the initial potential,  $[\text{Fe}(\text{CN})_6]^{4-}$  was oxidized into  $[\text{Fe}(\text{CN})_6]^{3-}$ , resulting in an oxidation current. The anode peak potential  $E_{pa}$  is 0.25 V (vs. SCE). According to Equation 2, the standard electrode potential of  $[\text{Fe}(\text{CN})_6]^{4-}-[\text{Fe}(\text{CN})_6]^{3-}$  redox pair is



In the actual test, the formal potential  $E_{1/2}$  is 0.43 V (vs. NHE), which is close to the theoretical value of 0.36 V, and the potential difference  $\Delta E_p$  is about 0.2 V. This shows the test of  $[\text{Fe}(\text{CN})_6]^{3-}$  by multiple response composite electrode is the process of quasi reversible reaction.

At the same time, as the concentration of  $[\text{Fe}(\text{CN})_6]^{3-}$  increases, the redox peak current in the CV curve gradually increases. The reduction peak current of the curve was linearly fitted with  $[\text{Fe}(\text{CN})_6]^{3-}$  concentration, and the results were shown in Fig.4 (e). Within the range of  $1.0\times 10^{-7}\sim 2\times 10^{-6}$  mol/L, the reduction peak current has a linear relationship with  $[\text{Fe}(\text{CN})_6]^{3-}$  concentration. The standard curve is as shown in the Fig, and the linear correlation coefficient is larger than 0.9950. ( $i_{pc}$  is the reduction peak current in  $\mu\text{A}$ ;  $c$  is the concentration of  $[\text{Fe}(\text{CN})_6]^{3-}$  in mmol/L). The detection limit of the composite electrode can be calculated according to Equation 3 [56]

$$\text{LOD} = 3.3 \sigma/s \quad \text{(Equation 3)}$$

( $\sigma$  is the standard deviation of the intercept and  $s$  is the slope of the curve.). Therefore, the detection limit of the  $[\text{Fe}(\text{CN})_6]^{3-}$  detectable multi-response nanocomposite electrode was 50.1  $\mu\text{M}$  which is higher than sensors in other reports [57].

By comparing the cyclic voltammetry curves of polymer composites with different block ratios, it can be found that with the increase of polyMAzo content in the multi-response block polymer, the redox peak current and the detection limit increase. Under visible light, the azobenzene group has a trans configuration and regular structure. Compared with the random group state of polyDMAEMA molecular chain, azophenyl group is more conducive for the penetration and reaction of ions [58,59]. The above analysis indicates that this electrode has good regularity for cyclic voltammetry of  $[\text{Fe}(\text{CN})_6]^{3-}$  and can be used for quantitative detection of  $[\text{Fe}(\text{CN})_6]^{3-}$  ion.

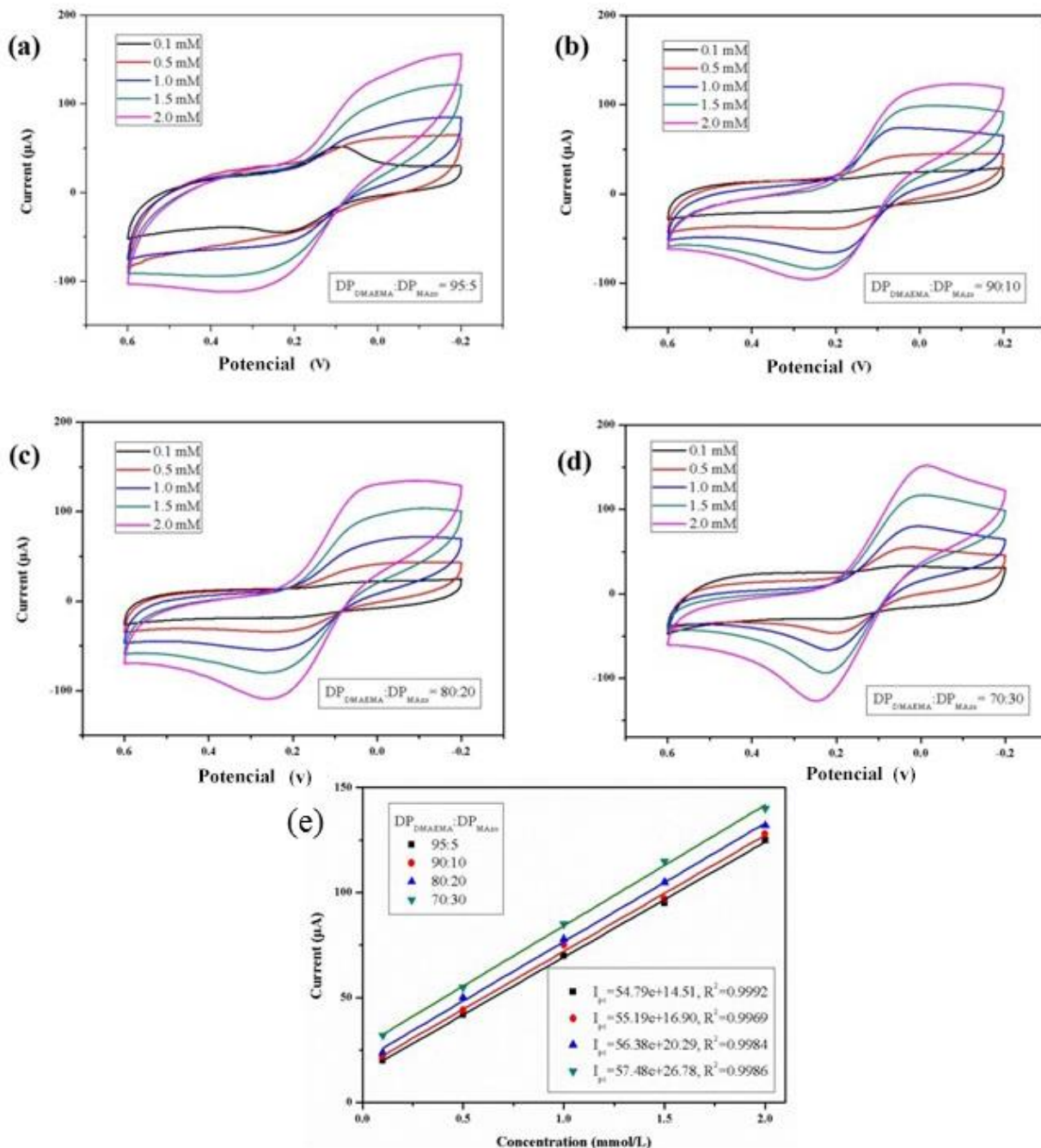


**Figure 4.** CV curves of various hybrid electrodes in different concentration of  $[\text{Fe}(\text{CN})_6]^{3-}$ , DP<sub>DMAEMA</sub>:DP<sub>MAzo</sub> is (a) 95:5, (b) 90:10, (c) 80:20 and (d) 70:30; (e) Response curves of various hybrid electrodes on  $[\text{Fe}(\text{CN})_6]^{3-}$ . The scanning rate is 50 mV/s. The electrolytes are  $[\text{Fe}(\text{CN})_6]^{3-}$  solution in different concentrations.

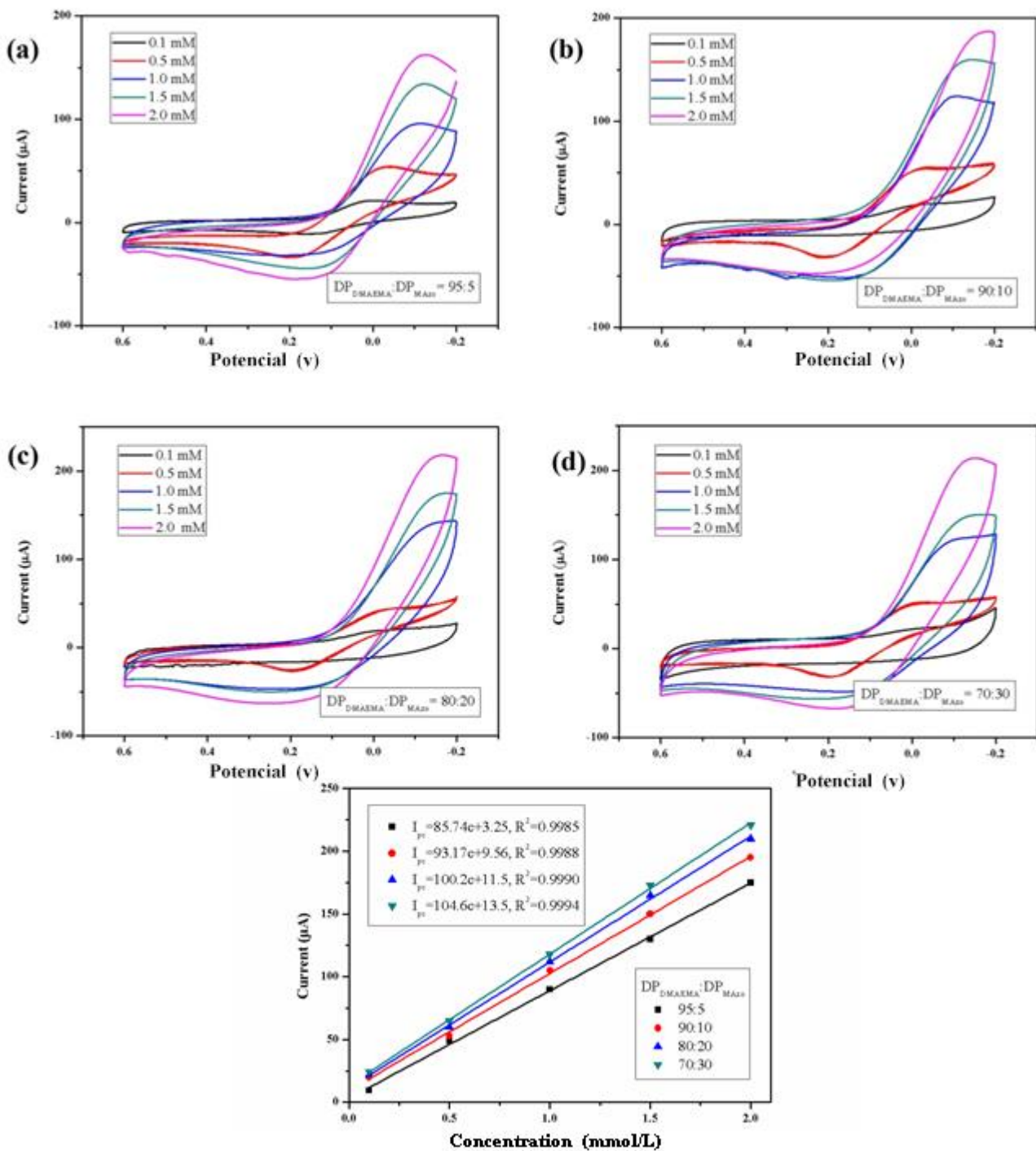


**Figure 5.** CV curves of various hybrid electrodes in different concentration of  $\text{Cu}^{2+}$ , DP<sub>DMAEMA</sub>:DP<sub>MAzo</sub> is (a) 95:5, (b) 90:10, (c) 80:20 and (d) 70:30; (e) Response curves of various hybrid electrodes on  $\text{Cu}^{2+}$ . The scanning rate is 50mV/s. The electrolytes are  $\text{Cu}^{2+}$  solution in different concentrations.

CV curves of a series of  $\text{Cu}^{2+}$  solution with different concentrations were tested by the multi-response composite electrode. The scanning rate is 50mV/s and the electrolytes are  $\text{Cu}^{2+}$  solution in different concentrations. The results are shown in Fig.5 (a)-(d). As can be seen from the figure, the cycle curve of  $\text{Cu}^{2+}$  is symmetrical, the reduction peak is obvious, and the oxidation peak is small,

indicating that some ions are partially adsorbed on the electrode. This phenomenon means the reaction is irreversible. When the initial potential (+ 0.6v) was scanned forward to the transition potential (-0.2v), Cu<sup>2+</sup> in the solution is reduced to Cu to generate the reduction current, and the cathode peak potential  $E_{pc}$  is -0.15 V (vs. SCE); From the negative scanning of the transition potential to the initial potential, Cu is oxidized to Cu<sup>2+</sup> to generate an oxidation current, and the anode peak potential  $E_{pa}$  is 0.10 V (vs. SCE). Equations 4 show the standard electrode potential of Cu<sup>2+</sup> - Cu redox pair [60-62].



In the actual test, the formal potential  $E_{1/2}$  is 0.26 V (vs. NHE), which is close to the theoretical value of 0.34 V, and conforms to the cyclic volt-ampere curve rule of Cu<sup>2+</sup>. The CV curve is not completely symmetrical, and  $i_{pc}/i_{pa} > 1$ , indicating that the process of testing Cu<sup>2+</sup> with the multi-response composite electrode is irreversible.

At the same time, with the increase of Cu<sup>2+</sup> concentration in the solution, the reduction peak current in the cyclic voltammetry curve increases significantly, while the oxidation peak current slightly increases. The reduction peak current of the curve was linearly fitted with the Cu<sup>2+</sup> concentration, and the standard curve was calculated. The result is shown in Fig.5 (e). It can be found that the peak current has a linear relationship with the Cu<sup>2+</sup> concentration in the range of  $1.0 \times 10^{-7} \sim 2 \times 10^{-6}$  mol/L. As shown in the figure, the linear correlation coefficient is small, and the detection limit is 47.2 μM. ( $i_{pc}$  is the reduction peak current, the unit is μA;  $c$  is the Cu<sup>2+</sup> concentration, the unit is mmol/L). By comparing the cyclic voltammetry curves of polymer composites with different block ratios, it can also be found that with the increase of polyMAzo content in the block polymer, the redox peak current and the detection limit increase. The above phenomenon indicates that the nanocomposite electrode has good regularity in detecting the cyclic voltammetry of Cu<sup>2+</sup>, and can be used for quantitative detection of Cu<sup>2+</sup>.

Under the same conditions, a series of different concentrations of Cd<sup>2+</sup> solutions were tested by composite electrodes. The results are shown in Fig.6 (a)-(d). As can be seen from the figure, the cyclic voltammetry curve of Cd<sup>2+</sup> is symmetrical and the redox peak is obvious. The cathode peak potential  $E_{pc}$  was -1.05 V (vs. SCE), and the anode peak potential  $E_{pa}$  was -0.85 V (vs. SCE). Equation 5 is the standard electrode potential of Cd<sup>2+</sup> - Cd redox pair [62-64]:



In the actual test, the formal potential  $E_{1/2}$  is -0.67 V (vs. NHE), which is close to the theoretical value of -0.40 V. The cyclic volt-ampere curve is basically symmetrical,  $i_{pc}/i_{pa} > 1$ , indicating that the process is a quasi-reversible reaction. At the same time, with the increase of Cd<sup>2+</sup> concentration in the solution, the reduction peaks current in the cyclic voltammetry curve increased significantly, while the oxidation peak current increased slightly. The reduction peak current of the curve was linearly fitted with the Cd<sup>2+</sup> concentration, and the standard curve was calculated. The results are shown in Fig.6 (e). It can be found that the peak current has a linear relationship with the concentration of Cd<sup>2+</sup> in the range of  $1.0 \times 10^{-7} \sim 2 \times 10^{-6}$  mol/L. As shown in the figure, the linear correlation coefficient is about 0.99, and the detection limit is 36.7 μM. ( $i_{pc}$  is the reduction peak current, the unit is μA;  $c$  is the concentration of Cd<sup>2+</sup>, the unit is mmol/L). At the same time, it was found that with the increase of polyMAzo content in the block polymer, the redox peak current and the

detection limit increased. The above phenomenon indicates that the nanocomposite electrode has good regularity for CV result of Cd<sup>2+</sup> and can be used for quantitative detection of Cd<sup>2+</sup>.

Compared with other reports [57,62,65,66], the detection limit of the sensor is higher, but it can be seen from the relationship between peak current and ion concentration that they have excellent linear relationship, which shows that the sensor can not only judge the existence of heavy metal ions, but also detect heavy metal ions quantitatively.

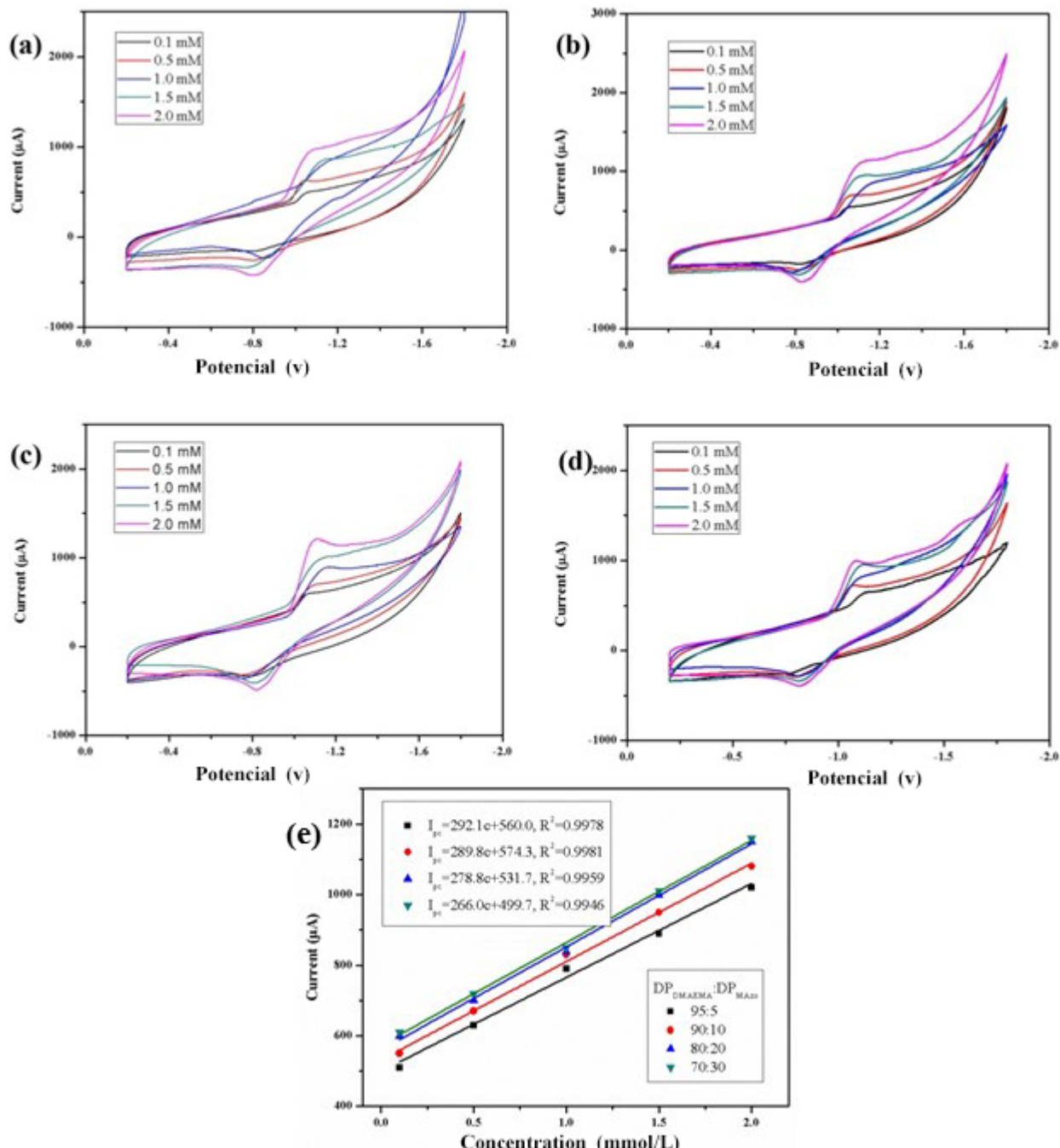


**Figure 6.** CV curves of various hybrid electrodes in different concentration of Cd<sup>2+</sup>, DP<sub>DMAEMA</sub>:DP<sub>MAzo</sub> is (a) 95:5, (b) 90:10, (c) 80:20 and (d) 70:30; (e) Response curves of various hybrid electrodes on Cd<sup>2+</sup>. The scanning rate is 50 mV/s. The electrolyte is Cd<sup>2+</sup> solution in different concentrations.

### 3.3 Multi-stimuli environmental responsibility

The introduction of multi-responsive polymer brush gives the composite electrode multi-stimuli environmental responsibility. In order to further explore the impact of responsibility on its detection performance, the  $[Fe(CN)_6]^{3-}$ ,  $Cu^{2+}$ ,  $Cd^{2+}$  solution under different pH, temperature, and ultraviolet (UV) conditions was tested by multi-responsive composite electrodes, respectively.

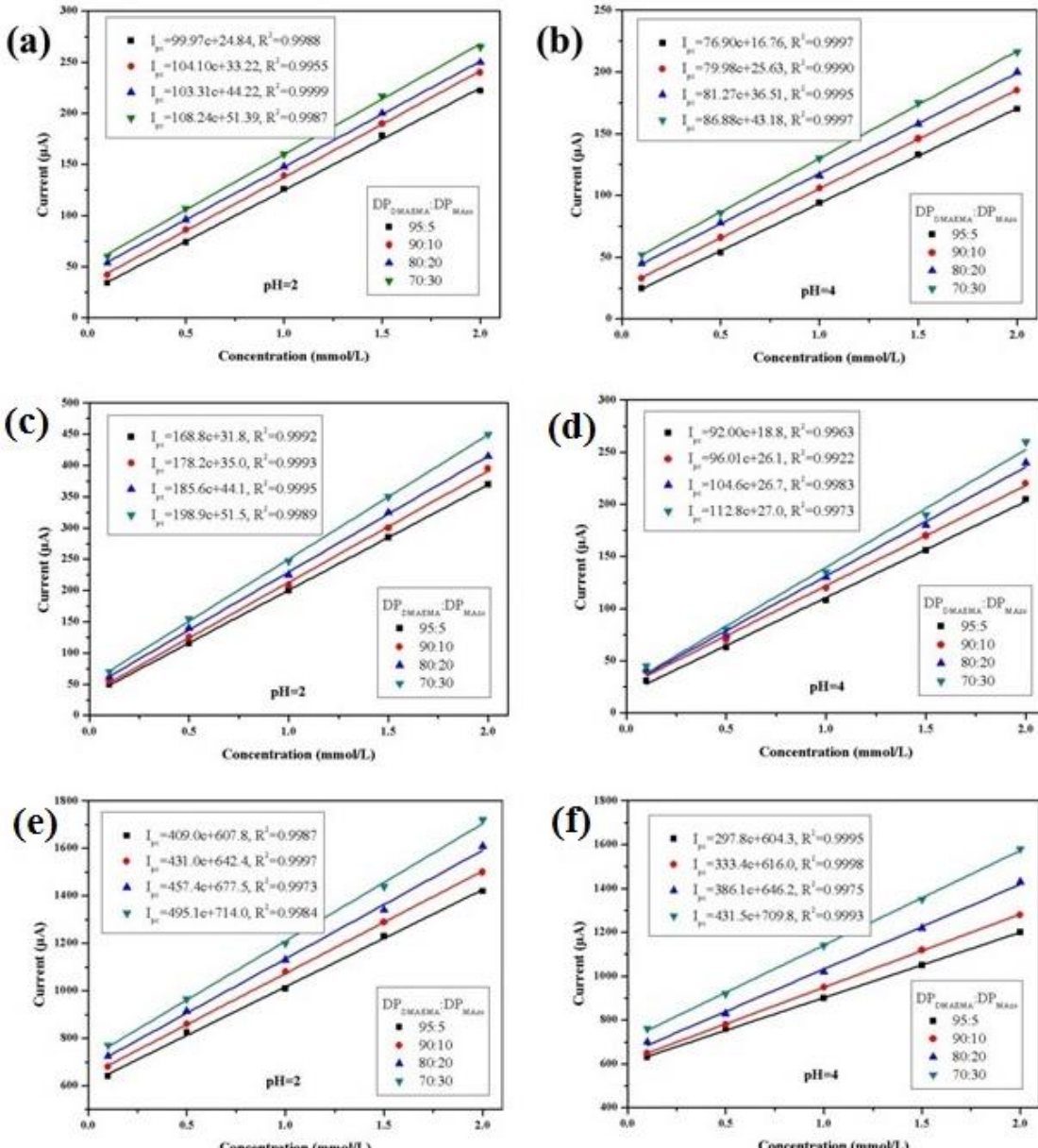


**Figure 7.** Response curves of various hybrid electrodes on  $[Fe(CN)_6]^{3-}$  ion at (a) pH 2 and (b) pH 4; on  $Cu^{2+}$  at (c) pH 2 and (d) pH 4; on  $Cd^{2+}$  at (e) pH 2 and (f) pH4. The scanning rate is 50 mV/s, electrolyte is 1mM metal ion solution.

According to the results, we got the standard curves shown in Fig.7 and Fig.8. Fig.7 shows the standard curve obtained at different pH values, where Fig.7 (a) and (b) are the standard curve of  $[Fe(CN)_6]^{3-}$ , Fig.7 (c) and (d) are the standard curve of  $Cu^{2+}$ , Fig.7 (e) and (f) are the standard curve of

$\text{Cd}^{2+}$ . It can be found that in the range of  $1.0 \times 10^{-7} \sim 2 \times 10^{-6}$  mol/L, the peak current has a linear relationship with the concentration of  $[\text{Fe}(\text{CN})_6]^{3-}$ . The detection limit of  $[\text{Fe}(\text{CN})_6]^{3-}$  at pH=2 was 20.4  $\mu\text{M}$  and when pH was 4, the limit was 34.5  $\mu\text{M}$ . The detection limit is 50.1  $\mu\text{M}$  in the neutral condition. The above phenomenon indicates that under acidic conditions, the test of  $[\text{Fe}(\text{CN})_6]^{3-}$  with multi-responsive composite electrode has better reversibility, and lower detection limit.

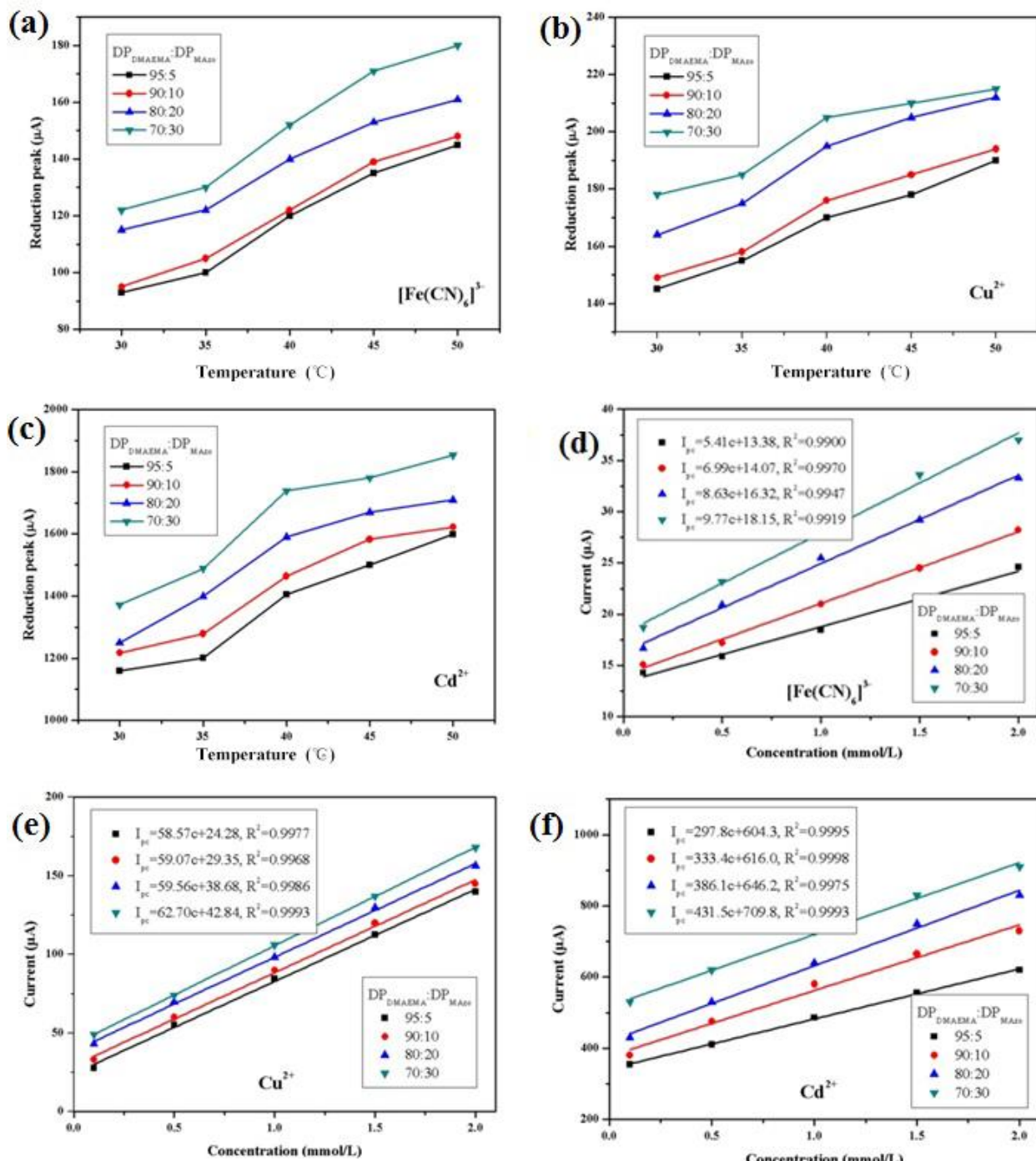


**Figure 8.** The reduction peak value of various hybrid electrodes as a function of temperature: (a)  $[\text{Fe}(\text{CN})_6]^{3-}$ , (b)  $\text{Cu}^{2+}$ , (c)  $\text{Cd}^{2+}$ . Standard curve of test ion for composite electrode after ultraviolet light irradiation: (d)  $[\text{Fe}(\text{CN})_6]^{3-}$ , (e)  $\text{Cu}^{2+}$ , (f)  $\text{Cd}^{2+}$ . The scanning rate is 50 mV/s.

This phenomenon is mainly affected by the PDMAEMA of the block polymer brush. When the pH is lower than pKa, the tertiary nitrogen in the polycation electrolyte pdmaema is quaternion due to protonation, which has obvious proton exchange with the solution, which is conducive to the penetration and reaction of ions on the electrode, and the oxidation-reduction peak current is large. When the pH is higher than pKa, the quaternary ammonium type tertiary nitrogen depolymerization is in the form of free amine, the polarity of molecular chain is small, the ion is difficult to penetrate the polymer brush, and the redox peak current is small [67,68].

From Fig.7 (c)-(f) we can see when pH is 2, the detection limit for  $\text{Cu}^{2+}$ ,  $\text{Cd}^{2+}$  are 17.9  $\mu\text{M}$  and 20.6  $\mu\text{M}$ , respectively, which data doubled the ions detection effect. Under acidic conditions, the block polymer brush is protonized, and easy to exchange with proton in the solution. Ions are easy to react on the surface of the electrode, and the reduction peak current is large. This phenomenon is similar to the detection results of  $[\text{Fe}(\text{CN})_6]^{3-}$ , which prove acid condition can significantly improve the detection limit of the composite electrode for ion detection.

Fig.8 (a)-(c) show the change of reduction peak current value obtained by CV test of 1 mM metal ions solution with the multi-responsive composite electrode at different temperatures. As can be seen from the figure, when the temperature increases, the redox peak current value increases. The polyDMAEMA block in the polymer brush is a cationic polyelectrolyte with both dual temperature and pH responsiveness, which also has a low critical solution temperature (LCST) phenomenon in the polymer chain structure [69]. When the temperature is lower than the LCST, the polymer chain is in a stretched state, the thickness of the polymer brush is large, which hinders the transport and reaction of ions on the electrode, so the reduction peak current is small. When the temperature is higher than LCST, the polymer chain is in a tortuous state, the polymer brush collapses, the thickness of the polymer brush is small, and the proton transport is relatively easy, so the redox peak current is large. According to Fig.8 (a)-(c), the polymer brush has an LCST of about 37 °C. At the same time, as the proportion of polyMAzo in the polymer brush increases, because of the conjugated structure of azobenzene, promoting the reaction and proton migration, the redox peak also increases. Besides, the redox peak of  $[\text{Fe}(\text{CN})_6]^{3-}$  is more variable than  $\text{Cu}^{2+}$  and  $\text{Cd}^{2+}$ . For the DP<sub>DMAEMA</sub>:DP<sub>MAzo</sub>=95:5 composite electrode, the reduction peak current increased from 92  $\mu\text{A}$  at 30 °C to 153  $\mu\text{A}$  at 50 °C, an increase of 65%. Since  $[\text{Fe}(\text{CN})_6]^{3-}$  reacts on the electrode, only one electron is transferred, and in the reaction of  $\text{Cu}^{2+}$  and  $\text{Cd}^{2+}$ , two electrons are transferred, so the redox peak current changes of  $[\text{Fe}(\text{CN})_6]^{3-}$  are most pronounced.

The composite electrode was tested for CV test of  $[\text{Fe}(\text{CN})_6]^{3-}$ ,  $\text{Cu}^{2+}$ ,  $\text{Cd}^{2+}$  after UV radiation. The standard curve for reducing peak current is shown in Fig.8 (d)-(f). As can be seen from the figure, after ultraviolet radiation, the redox peak of the cyclic voltammetry curve of the composite electrode is significantly reduced, the detection limit is lowered, and the detection ability is limited. This phenomenon is mainly affected by the polyMAzo portion in the polymer brush [49,70]. Under visible light conditions, the azobenzene group of the polyMAzo segment is a stable trans configuration with a small inter-molecular distance and no polarity. The ions are more permeable to the polymer brush to the surface of the electrode. The redox peak current is large. Under ultraviolet light conditions, the azobenzene group changes from a trans structure to a cis structure, and the polarity is large. The molecular chains are entangled together, hindering the transport and reaction of ions on the electrode

surface, and the redox peak current value. This phenomenon indicates that the ultraviolet-visible light can function as a switch that regulates the detection capability of the composite electrode.

#### 4. CONCLUSIONS

Based on the mesoporous silica SBA-15 framework, the multi-responsive block polymer brush PMAzo-PDMAEMA-SBA-15 was modified by SI-RAFT method. The specific surface area and pore diameter of the composites modified by polymer brush were reduced, but the morphology of mesoporous structure was maintained. The detection performance of  $[Fe(CN)_6]^{3-}$ ,  $Cu^{2+}$ ,  $Cd^{2+}$  was studied by CV analysis. The CV curve of the nanocomposite electrode has obvious redox peak, and the peak current has a linear relationship with the square root of the scanning speed when the scanning speed is 50 mV/s. In the range of  $1.0 \times 10^{-7} \sim 2 \times 10^{-6}$  mol/L, the reduction peak current of CV curves has a linear relationship with the concentration of  $[Fe(CN)_6]^{3-}$ ,  $Cu^{2+}$ ,  $Cd^{2+}$  ions, and the linear correlation is very high and can be used for quantitative analysis of ions. The multi-stimuli environmental response characteristics have an impact on its detection performance. The decrease of pH and the increase in temperature increase the peak value of redox, which improves the sensitivity and detection limit of ion detection. At the same time, it was found that after ultraviolet light, the redox peak current of the composite electrode was significantly reduced, and the ultraviolet-visible light could play a role in regulating the switch.

#### ACKNOWLEDGEMENT

F. Chen thanks the financial support of Natural Science Foundation of Zhejiang Province, China (No. LY19E030007) and Surfactants Key Enterprise Laboratory of Zhejiang Province, Zanyu Technology Group Co., LTD.

#### References

1. F. Fu, Q. Wang, *Journal of Environmental Management*, 92(2011)407.
2. J. Lars. *British Medical Bulletin*, 68(2003)167.
3. K. E. Giller, E. Witter and S. P. McGrath, *Soil Biol. Biochem.*, 30(1998)1389.
4. M. Valko, H. Morris and M. Cronin, *Curr. Med. Chem.*, 12 (2005)1161.
5. K. Jomova, M. Valko, *Toxicology*, 83 (2011)65.
6. H. N. Kim, W. X. Ren and J. S. Kim, *Chemical Society Reviews*, 41 (2012)3210.
7. V. K. Gupta, M. R. Ganjali and P. Norouzi, *Crit. Rev. Anal. Chem.*, 41(2011)282.
8. C. C. Huang, H. T. Chang, *Anal. Chem.*, 8(2006)8332.
9. G. K. Darbha, A. K. Singh and U. S. Rai, *J. Am. Chem. Soc.*, 130(2008)8038.
10. Z. P. Zhao, Z. P. Zhou and M. Q. Zhong, *Int. J. Electrochem. Sci.*, 9(2014)8120.
11. Z. P. Zhao, Z. P. Zhou and J. B. Ji, *Int. J. Electrochem. Sci.*, 10(2015)4303.
12. Z. P. Zhao, Z. P. Zhou and M. Q. Zhong, *Int. J. Electrochem. Sci.*, 10(2015)5026.
13. Z. P. Zhao, Z. P. Zhou and M. Q. Zhong, *Int. J. Electrochem. Sci.*, 12(2017)5450.
14. S. Zeng, K. T. Yong and I. Roy, *Plasmonics*, 6(2011)491.
15. M. B. Gumpu, S. Sethuraman and U. M. Krishnan, *Sens. Actuators, B*, 213(2015)515.

16. T. Asefa, M. J. MacLachlan, *Nature*, 402 (1999)867.
17. S. Chui, S. Lo and Charmant, *Science*, 283 (1999)1148.
18. X. K. Li, J. Liu and F. L. Du, *Appl. Surf. Sci.*, 464(2019)21.
19. B. Y. Xia, Y. Yan and N. Li, *Nature energy*, 1(2016)15006.
20. L. Liao, S. N. Wang and J. J. Xiao, *Energy & environmental science*, 7(2014)387.
21. T. R. Kuang, L.Q. Chang and X. F. Peng, *Trends Biotechnol.*, 35(2017)347.
22. J. Liu, N. P. Wickramaratne and S. Z. Qiao, *Nat. Mater.*, 14(2015)763.
23. K. Ariga, A. Vinu and Y. Yamauchi, *Cheminform*, 85(2012)1.
24. J. Peng, X. Zhao and W. Wang, *Langmuir*, 35(2019)8404.
25. X. J. Wei, J. Shen and F. Chen, *ACS Applied Bio Materials*, 1(2018)2167.
26. A. Corma, *Chem. Rev.*, 97(1997)2373.
27. S. H. Joo, S. J. Choi and I. Oh, *Nature*, 412(2001)169.
28. M. M. Jin, Z. M. Guo and Z. G. Lv, *J. Mater. Sci.*, 54(2019)6853.
29. L. B. Desmonts, N. D. Reinhoudt, *Chem. Soc. Rev.*, 6(2007)993.
30. I. I. Slowing, B. G. Trewyn and S. Giri, *Adv. Funct. Mater.*, 17(2007)1225.
31. V. Biju, *Chem. Soc. Rev.*, 43(2013)744.
32. X. Huang, X. Teng and D. Chen, *Biomaterials*, 31(2010)438.
33. A. M. Chen, M. Zhang and D. G. Wei, *Small*, 5(2010)2673.
34. T. H. Chung, S. H. Wu and M. Yao, *Biomaterials*, 28(2007)2959.
35. Y. Z. Zhu, J. Shen and F. Chen, *Chem. Eng. J.*, 366(2019)112.
36. S. Mura, J. Nicolas, *Nat. Mater.*, 12(2013)991.
37. J. Kim, H. S. Kim and N. Lee, *Angew. Chem. Int. Ed.*, 47(2008)8438.
38. J. L. Vivero-Escoto, I. I. Slowing and B. G. Trewyn, *Small*, 6 (2010)1952.
39. J. Lu, M. Liong and Z. Li, *Small*, 6(2010)1794.
40. B. Jaleh, S. Ghasemi and M. J. Torkamany, *Appl. Surf. Sci.*, 427(2018)640.
41. M. G. Álvarez, R. J. Chimentão and D. Tichit, *Micropor. Mesopor. Mat.*, 219(2016)19.
42. M. Vallet-Regí, F. Balas and D. Arcos, *Angew. Chem. Int. Ed.*, 46(2007)7548.
43. S. H. Joo, J. Y. Park and C. K. Tsung, *Nat. Mater.*, 8(2009)126.
44. F. Chen, X. P. Jiang, T. R. Kuang, *RSC Advances*, 5(2015)70204.
45. F. Chen, X. P. Jiang, T. R. Kuang, *Polym. Chem.*, 6(2015)3529.
46. H. Yoshioka, C. Izumi and M. Shida, *Polymer*, 119(2017)167.
47. F. Chen, Y. Z. Zhu and W. Li, *Appl. Surf. Sci.*, 464(2019)273.
48. F. Chen, D. X. Dai, J. T. Yang, *J. Macromol. Sci. A: Pure Appl. Chem.*, 50(2013)1002.
49. W. Li, T. R. Kuang, X. Jiang, *Chem. Eng. J.*, 322(2017) 445.
50. Z. P. Zhao, Z. P. Zhou and L. X. Xue, *Int. J. Electrochem. Sci.*, 13(2018)925.
51. Z. P. Zhao, C. Y. Pan, G. J. Jiang, *Int. J. Electrochem. Sci.*, 13(2018)2945.
52. Z. P. Zhao, Z. P. Zhou and M. Q. Zhong, *Int. J. Electrochem. Sci.*, 13(2018)3621.
53. Z. P. Zhao, Z. C. He and Z. P. Zhou, *Int. J. Electrochem. Sci.*, 13(2018)4018.
54. T. S. Anirudhan, J.R. Deepa, *Mat. Sci.eng. C.*, 92(2018)942.
55. S. Deshmukh, G. Kandasamy, R.K., *J. Electroanal. Chem.*, 788 (2017) 91.
56. L. H. Tang, Y. Wang, Y.M. Li, *Adv. Funct. Mater.*, 19(2019)2782.
57. T. A. Ali, G. G. Mohamed, A. H. Farag, *Int. J. Electrochem. Sci.*, 10 (2015) 564.
58. A. Natansohn, P. Rochon, *Chem. Rev.*, 102 (2002) 4139.
59. E. W. G. Diau, *J. Phys. Chem. A*, 108 (2004) 950.
60. Y. Wei, C. Gao, F. L. Meng, *J. phys. chem. C*, 116 (2012) 1034.
61. W.J. Li, X.Z. Yao, Z. Guo, *J. Electroanal. Chem.*, 749 (2015) 75
62. X. Li, H. Wen, Q. Fu, *Appl. Surf. Sci.*, 363 (2016) 7.
63. L. Liu, K. Zhuo, Z. Y. Yuan, *Int. J. Electrochem. Sci.*, 14 (2019) 5317.
64. L. Liu, C. Yu, X. X. Zhang, *Int. J. Electrochem. Sci.*, 14 (2019) 4469.
65. X. Z. Zhang, K. M. Qu, D.P. Li, *Int. J. Electrochem. Sci.*, 10 (2015) 8497.

66. H. M. Wang, C. Y. Xu, B. Q. Yuan, *Int. J. Electrochem. Sci.*, 14 (2019) 8760.
67. W.J. Guo, T.S. Wang, X.D. Tang, *J. Polym. Sci. Polym. Chem.* 52 (2014) 2131.
68. E.H. Otal, P.C. Angelome, S.A. Bilmes, *Adv. Mater.* 18(2006) 934.
69. D. Fournier, R. Hoogenboom, H.M.L. Thijs, R.M. Paulus, *Macromolecules* 40 (2007) 915.
70. W.J. Guo, T.S. Wang, X.D. Tang, Q. Zhang, F.Q. Yu, *J. Polym. Sci. Polym. Chem.* 52 (2014) 2131.

© 2020 The Authors. Published by ESG ([www.electrochemsci.org](http://www.electrochemsci.org)). This article is an open access article distributed under the terms and conditions of the Creative Commons Attribution license (<http://creativecommons.org/licenses/by/4.0/>).